Biosensors and Bioelectronics 24 (2009) 3556–3561

Contents lists available at ScienceDirect

Biosensors and Bioelectronics

journal homepage: www.elsevier.com/locate/bios

Xanthine oxidase/laponite nanoparticles immobilized on glassy carbon electrode: Direct electron transfer and multielectrocatalysis

Dan Shan[a,*], Yan-Na Wang[a], Huai-Guo Xue[a,*], Serge Cosnier[b], Shou-Nian Ding[b,c]

[a] College of Chemistry & Chemical Engineering, Yangzhou University, Jiangsu 225002, China
[b] Département de Chimie Moléculaire UMR-5250, ICMG FR-2607, CNRS Université Joseph Fourier, BP-53, 38041 Grenoble, France
[c] School of Chemistry & Chemical Engineering, Southeast University, Nanjing 211189, China

ARTICLE INFO

Article history:
Received 21 January 2009
Received in revised form 17 April 2009
Accepted 11 May 2009
Available online 18 May 2009

Keywords:
Xanthine oxidase
Laponite
Xanthine
Direct electrochemistry
Nitrate
Biosensor

ABSTRACT

In this work, colloidal laponite nanoparticles were further expanded into the design of the third-generation biosensor. Direct electrochemistry of the complex molybdoenzyme xanthine oxidase (XnOx) immobilized on glassy carbon electrode (GCE) by laponite nanoparticles was investigated for the first time. XnOx/laponite thin film modified electrode showed only one pair of well defined and reversible cyclic voltammetric peaks attributed to XnOx–FAD cofactor at about −0.370 V vs. SCE (pH 5). The formal potential of XnOx–FAD/$FADH_2$ couple varied linearly with the increase of pH in the range of 4.0–8.0 with a slope of −54.3 mV pH^{-1}, which indicated that two-proton transfer was accompanied with two-electron transfer in the electrochemical reaction. More interestingly, the immobilized XnOx retained its biological activity well and displayed an excellent electrocatalytic performance to both the oxidation of xanthine and the reduction of nitrate. The electrocatalytic response showed a linear dependence on the xanthine concentration ranging from 3.9×10^{-8} to 2.1×10^{-5} M with a detection limit of 1.0×10^{-8} M based on S/N = 3.

1. Introduction

Xanthine oxidase catalyzes the oxidation of hypoxanthine to xanthine and can further catalyze the oxidation of xanthine to uric acid. Thus, this enzyme plays an important role in the catabolism of purines in some species, including human (Hille, 2005; Harrison, 2002). Since hypoxanthine and xanthine are the key indicators for estimating fish freshness and human health, XnOx has been implicated as a key oxidative enzyme by electrochemists to construct electrochemical sensors for the determination of hypoxanthine and xanthine, providing a simple, fast and reliable proposed systems (Kilinc et al., 1998; Rahman et al., 2007; Villalonga et al., 2007; Kirgöz et al., 2004; Zhao et al., 1996; Shan et al., 2009a; Shan et al., 2009b). Generally, the electrochemical detection of hypoxanthine or xanthine was based on the electrochemical oxidation of the enzymatically generated H_2O_2 and uric acid, or the electrochemical reaction of the introduced redox mediators. Obviously, the analytical performance was not satisfactory enough, especially due to the poor selectivity and stability.

The most promising approach for the development of electrochemical biosensors is to establish a direct electrical communication between the biomolecules and the electrode surface (Freire et al., 2003), which can avoid the use of redox mediators, thus reducing side reactions and potential interferences, as well as being more compatible with in vivo conditions. Nevertheless, the direct electron transfer reaction of XnOx is still very difficult to be achieved due to the deeply hided electro-active centers, thus rare reports appeared in the literatures (Bernhardt et al., 2006; Wang and Yuan, 2004; Zhou et al., 2006; Wu and Hu, 2007). Furthermore, previous attempts at direct electrochemically driven catalysis of this enzyme have been ineffective, due to the protein denaturation and unfavorable interactions (Bernhardt et al., 2006; Wang and Yuan, 2004).

Direct electron transfer of protein depends strongly on the immobilization procedure, the nature of the support, and the properties and the stability of the biomolecule (Freire et al., 2003). Clay colloid provides a favorable microenvironment for electron transfer and catalytic reactions on electrode (Shumyantseva et al., 2005; Liu et al., 2005a,b). In the literature, there are several reports on direct electrochemistry based on clay–protein modified electrode (Sun, 2006; Zhou et al., 2002; Li and Hu, 2003; Shan et al., 2007).

Laponite (hydrous sodium lithium magnesium silicate) is an entirely synthetic crystalline layered silicate colloid with crystal structure and composition closely resembling the natural smectite clay hectorite (Cummins, 2007). Individual particles are disk-shaped crystals, 25 nm in diameter and 1 nm in thickness, with chemical composition of $(Mg_{5.5}Li_{0.5})Si_4O_{10}(OH)_2(Na^+_{0.73}{\cdot}nH_2O)$,

* Corresponding authors. Tel.: +86 514 87975590 9519; fax: +86 514 87975244.
E-mail addresses: danshan@yzu.edu.cn (D. Shan), chhgxue@yzu.edu.cn (H.-G. Xue).

0956-5663/$ – see front matter © 2009 Elsevier B.V. All rights reserved.
doi:10.1016/j.bios.2009.05.009

significantly smaller than naturally occurring clays (Van Olphen, 1977). Within a single crystal, each sheet of octahedrally coordinated aluminum or magnesium oxide is sandwiched between two layers of tetrahedrally coordinated silica. An isomorphic substitution of magnesium by lithium atoms generates negative charge on its surface, which is counterbalanced by the positive charge of the sodium ions present in the interlayer. In an aqueous medium, sodium ions dissociate which, in turn, leads to a net negative charge on its surface. The edge of the laponite particle is composed of hydrous oxide, and depending on the pH of the solution, it appears that the sides of the disks can be charged positively (Van Olphen, 1977; Bonn et al., 1999). Its suspension in the aqueous medium leads to the formation of nonergodic soft solids that exhibit a rich variety of physical behavior (Joshi et al., 2008). Thus, laponite has been successfully used in the past as cast films onto electrodes for immobilization of redox proteins (Cosnier and Le Lous, 1996; Senillou et al., 1999; Mousty et al., 2001; Shan et al., 2002, 2003; Cosnier et al., 2006; Fan et al., 2007; Shan et al., 2003; Shi et al., 2008).

In this work, we continue to take advantage of the merit of laponite described above and attempt to design a novel third-generation biosensor based on immobilization of XnOx with colloidal laponite nanoparticles. Direct electron transfer and bioelectrocatalytic activity of immobilized protein were investigated by cyclic voltammetry and amperometry techniques. The XnOx/laponite film exhibits the feasibility in electrochemical catalysis towards xanthine and nitrate.

2. Experimental

2.1. Materials

Xanthine oxidase (XnOx) (EC1.1.3.22, from microbial source, 8.1 U mg^{-1}) was obtained from Sigma. Laponite is a synthetic hectorite (monovalent cation exchange capacity: CEC = 0.74 mmol g^{-1}) purchased from Laportes Industries.

All other reagents were of analytical grade and used as received without further purification. All aqueous solutions were prepared in deionized distilled water. Phosphate buffer solution (PBS) was 0.1 M Na_2HPO_4 and NaH_2PO_4 and its pH was adjusted with H_3PO_4 or NaOH solutions.

2.2. Measurements and apparatus

Atomic force microscopy (AFM) images were obtained with a multimode digital instrument (Vecco-DI). Static contact angle measurements were performed at 20 °C with a sessile drop method using an OCA 40 system (German). A droplet of deionized water (3 μl) or diiodomethane, CH_2I_2 (1.5 μl) was gently placed onto the surface. The angle between the edge of the droplet and the surface was measured. Measurements were made in different regions on the surface. A CHI 660 electrochemical workstation (CHI Co., USA) was used for cyclic and amperometric voltammetry. All electrochemical studies were performed with a conventional three-electrode system. A saturated calomel electrode (SCE) and a Pt foil electrode were used as reference electrode and counter electrode, respectively. The working electrode was a glassy carbon electrode (GCE) (diameter 3 mm), polished carefully with 0.05 μm alumina particles on silk followed by rinsing with the distilled water and dried in air before use. Unless otherwise indicated, electrolytic solutions were purged with highly purified nitrogen for at least 20 min prior to the series of experiments. The electrochemical experiments in aqueous solutions were performed under a nitrogen atmosphere.

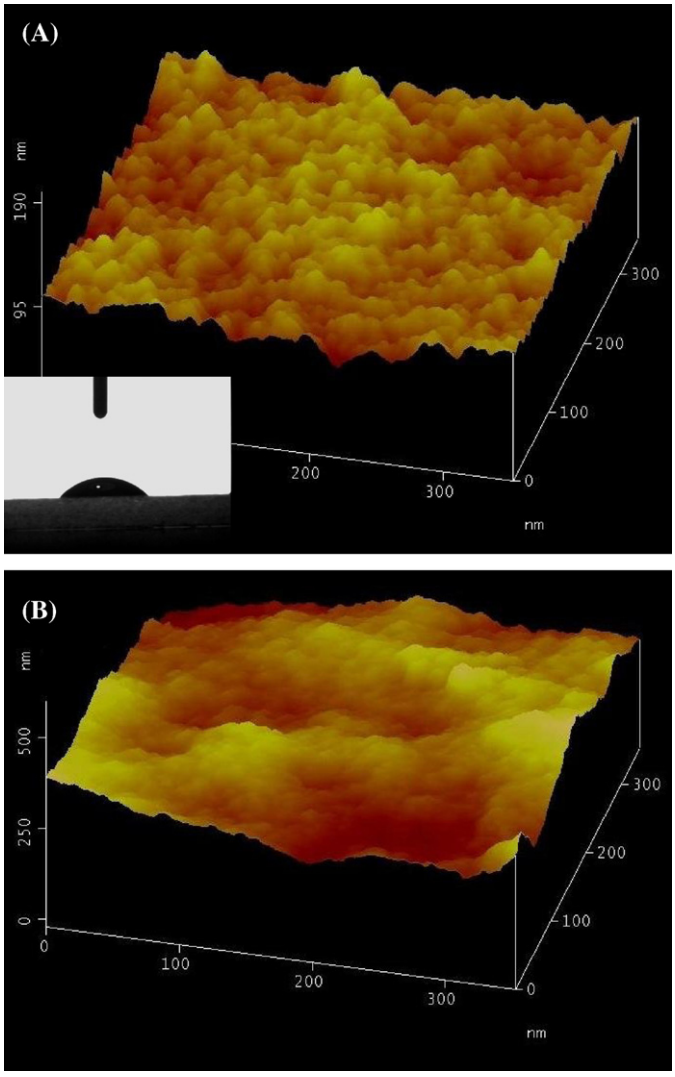

Fig. 1. Tapping mode AFM topography images of: (A) laponite film and (B) XnOx/laponite (w/w, 3/4) film on glassy carbon. Inset (A) shows the image of the initial droplet on laponite film.

2.3. Preparation of enzyme electrodes

The laponite colloidal suspension (2 mg ml^{-1}) was prepared by dispersing laponite in the deionized water with stirring overnight. XnOx was also dissolved in deionized water with a concentration of 2 mg ml^{-1}. A defined amount of aqueous XnOx/laponite mixture (for instance, containing 12 μg XnOx, 16 μg laponite) was spread on the surface of GCE. The mixture was dried in air at room temperature, leading to an adherent laponite film in which enzymes were entrapped. Before use, the enzyme electrode was rinsed under stirring for 20 min with buffer solution to remove the enzyme not firmly immobilized.

3. Results and discussion

3.1. Atomic force microscopy characterization

Topographical characterization was conducted using AFM in tapping mode. Fig. 1 shows surface topography images of laponite thin film and XnOx/laponite thin film, respectively. Fig. 1 A reveals the characteristic rag-like surface with domains of ridges and valleys formed by the deposition and the imperfect stacking of colloidal laponite nanoparticles on glassy carbon. The thickness of this

thin laponite film was 18.5 nm. As shown in Fig. 1B, the surface topography image of XnOx/laponite thin film changes a lot compared to Fig. 1A, since the heterocoagulation of XnOx and colloidal particles changes the surface characteristic of laponite thin film. The thickness of the XnOx/laponite thin film was 83.5 nm.

Inset of Fig. 1 A displays the image of the initial droplet on laponite thin film. The contact angle of laponite thin film was measured to be $48.8 \pm 0.4^{\circ}$, indicative for a hydrophilic surface. The highly hydrophilic laponite matrix can provide a favorable microenvironment to the immobilized protein. Measuring the contact angle between laponite film and two liquids of different polarity (deionized water and diiodomethane) can also provide the important information on surface energy, a fundamental material property that often affects biological interaction. Using the equation of geometric mean (Owens–Wendt–Kaelble approximation) (Ma et al., 1998), surface energy of laponite was calculated to be 56.84 J/m^2. The high surface free energy of laponite nanoparticles can make XnOx inevitably be adsorbed on the surface of nanoparticles. This strong driving force may lead to the specific orientation of the proteins and exposition of their active sites during the adsorption process.

3.2. Direct electrochemistry of XnOx at the laponite-modified GCE

The electrochemical properties of XnOx/laponite/GCE were studied by cyclic voltammetriy (CV). Fig. 2A shows the CVs of different electrodes in 0.1 M PBS (pH 5.0). The XnOx/laponite/GCE exhibits a couple of stable and well-defined redox peaks at scan rate of 150 mV s^{-1} (curve a in Fig. 2A). The anodic peak potential (E_{pa}) and cathodic peak potential (E_{pc}) are located at −0.357 and −0.386 V vs. SCE, respectively. The peak potential separation (ΔE_p) is 29 mV and the formal potential $E^{0\prime}$ (defined as the average of E_{pa} and E_{pc}) is −0.370 V. These peaks resulted from direct electron transfer of the immobilized XnOx attributed to the conversion of XnOx (FAD) to XnOx ($FADH_2$), which are consistent with values reported in the literatures for free FAD and the FAD redox center of the flavoenzyme (Rodrigues and Wedd, 1991; Wang and Yuan, 2004). However, no redox peak was observed at both bare GCE (curve b in Fig. 2A) and laponite/GCE (curve c in Fig. 2B). Thus, laponite must have a great effect on the kinetics of the electrode reaction for XnOx and provides a suitable microenvironment for the protein to transfer electrons with underlying GCE. It might be due to the strong driving force of laponite nanoparticles resulting from its high surface energy, which inducing the restricted orientations favorable to the direct electron transfer between the protein molecules and the underlying electrode.

Furthermore, this electrochemical signal is quite stable: the peak height and peak potential remains nearly unchanged. The XnOx/laponite/GCE was stored in pH 5.0 PBS, and during the whole storage time and CV tests were carried out periodically. The bioelectrode exhibited excellent long-term stability: the CV peak potentials kept the same positions and the peak currents retained 84% of their values for 20 days. Reproducibility of the XnOx/laponite/GCE fabrication was evaluated by CVs via the comparison of the peak currents of XnOx/laponite/GCE in 0.1 M PBS (pH 5.0) at scan rate of 150 mV s^{-1}. Twelve different bioelectrodes were tested independently; an average cathodic peak current was 0.83 μA providing the RSD values of 1.2%.

XnOx is a large and one of the most complex flavoproteins, and has potential multi electrochemical active centers (a molybdenum (VI) center, two iron–sulfur (Fe2–S2) clusters called Fe/S I and Fe/S II and a flavin adenine dinucleotide (FAD) unit) (Liu et al., 2005a,b). The CVs exhibits only the redox signal of FAD at the proposed XnOx/laponite/GCE. There are many reasons that might account for this phenomenon. The voltammetric experiment requires the protein to be confined to the electrode surface, and conformational

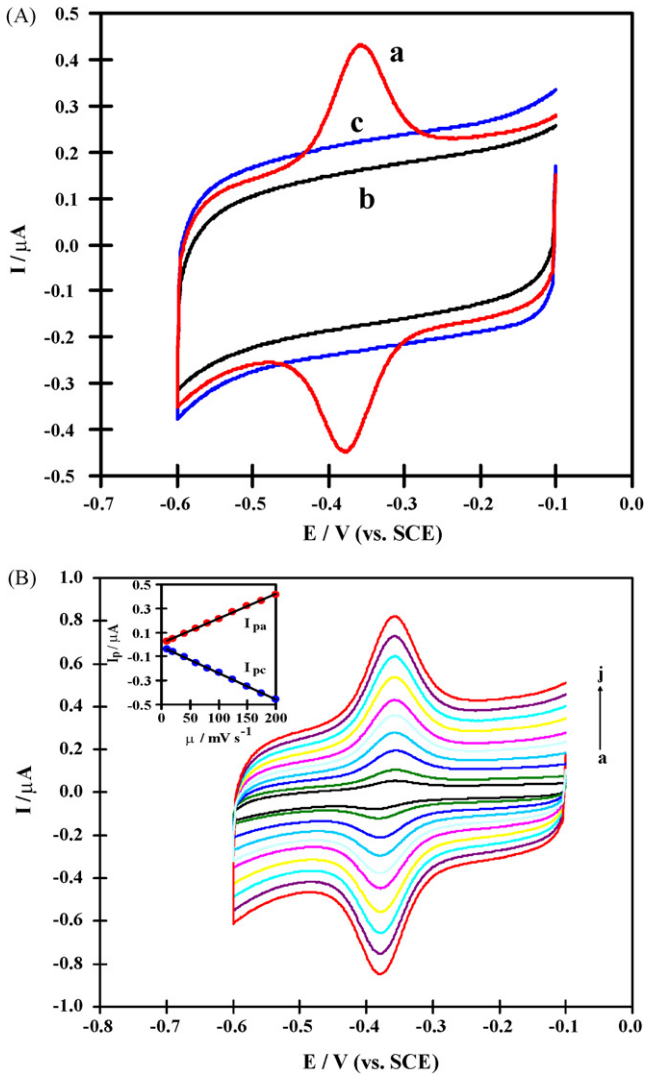

Fig. 2. (A) Cyclic voltammograms of (a) XnOx/laponite/GCE, (b) GCE and (c) laponite/GCE in 0.1 M PBS (pH 5.0) at scan rate of 150 mV s^{-1}. (B) Cyclic voltammograms of XnOx/laponite/GCE in 0.1 M PBS (pH 5.0) at different scan rates. The scan rate from inner to outer are (a) 10, (b) 20, (c) 40, (d) 60, (e) 80, (f) 100, (g) 125, (i) 150 and (j) 200 mV s^{-1}, respectively. Inset: The plot of anodic and cathodic peak currents vs. scan rate.

changes upon adsorption may result in different apparent redox potentials. The FAD group can exchange electron with electrode, because the active center has cave connecting to the protein surface. Fe2–S2 centers bury in the protein framework and act as wire conduction the electron transfer between FAD and molybdenum groups. In addition, the voltammetry does not offer the excellent resolution of different redox centers, besides the FAD, Fe2–S2 clusters, and Mo centers exhibiting quite similar potentials, thus considerable overlap can be seen in the corresponding voltammetry experiments.

The cyclic voltammogram of XnOx/laponite/GCE displays a well-defined peak shape at different scan rates (Fig. 2B). Peak currents vary linearly with the scan rates, as shown in the inset of Fig. 2B, indicating a surface-controlled electrode process. According to the slope of the I_p–ν curve and following the equation (Laviron, 1979):

$$I_p = \frac{n^2F^2\nu A\Gamma^*}{4RT} = \frac{nFQ\nu}{4RT}$$

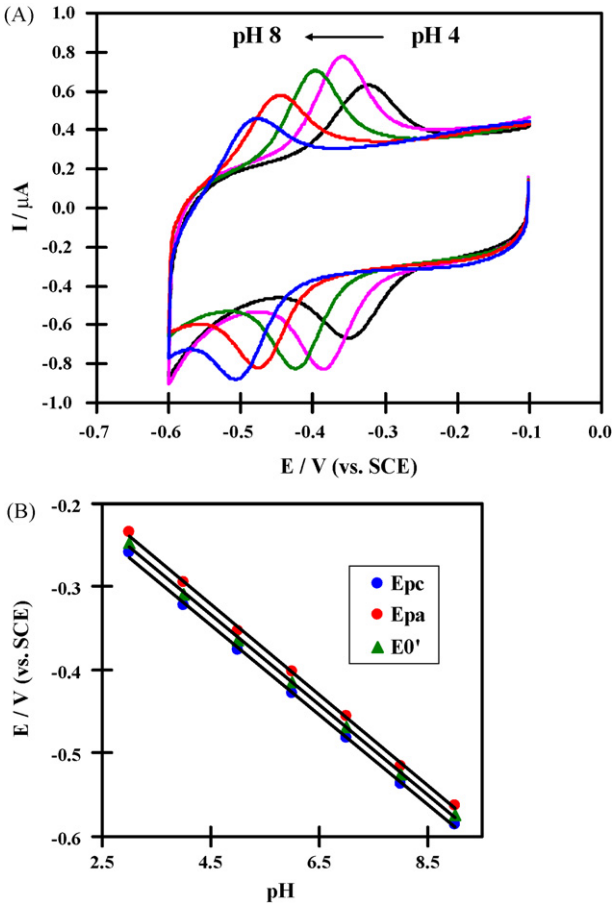

Fig. 3. (A) Cyclic voltammograms of XnOx/laponite/GCE in different of 4, 5, 6, 7 and 8; scan rate: 150 mV s^{-1}. (B) The effect of pH on E_{pa}, E_{pc} and the formal potential $E^{0'}$ of XnOx/laponite/GCE in 0.1 M PBS.

n is calculated as 2.1, meaning that 2e transfer is involved. At the same time, the I_{pa}/I_{pc} ratio and the formal potential $E^{0'}$ ($E^{0'} = (E_{pa} + E_{pc})/2$) keep almost unchanged, which are the typical characteristics of a reversible system. The average surface coverage (Γ^*) of the electro-active XnOx adsorbed on laponite nanoparticles is calculated to be 7.62×10^{-12} mol cm^{-2} from the slope of the I_p–ν curve. Considering the crystallographic size of XnOx of $116.3 \times 164.4 \times 153.2$ Å (Eger et al., 2000) and assuming that the XnOx molecule has a sphere shape with average diameter of 12.0 nm, the theoretical value for the monomolecular layer of XnOx on the bare electrode surface was calculated to be 1.47×10^{-12} mol cm^{-2} (geometric area of the electrode surface was taken). The obtained value of Γ^* is about 5 times as large as the theoretical monolayer coverage. This implies that a multilayer of XnOx participated in the electron transfer process.

3.3. Effect of pH on the direct electron transfer of immobilized XnOx

Generally, the $E^{0'}$ of the redox couple depends on solution pH which indicates the participation of proton in the redox process. Fig. 3A depicts a series of cyclic voltammograms recorded at XnOx/laponite/GCE in PBS exhibiting different pH values. It appears that an increase in pH from pH 4.0 to 8.0 led to a negative shift of both oxidation and reduction peak potentials. The linear regression equation is $E^{0'} = -0.0887 - 0.0543$pH (r = 0.9992) (Fig. 3B). The value of the slope (−54.3 mV pH^{-1}) value is approximately close to the theoretical value of −59 mV pH^{-1} expected for a proton/electron ratio of 1.0. As other FAD-containing flavoenzymes, the direct electrochemistry of XnOx on the laponite modified electrode is a two-proton coupled with two-electron redox reaction process. Thus, the direct electrochemical reaction could be described as below:

$$\mathrm{XnOx - FAD} + 2e^- + 2\mathrm{H}^+ \rightleftharpoons \mathrm{XnOx - FADH_2}$$

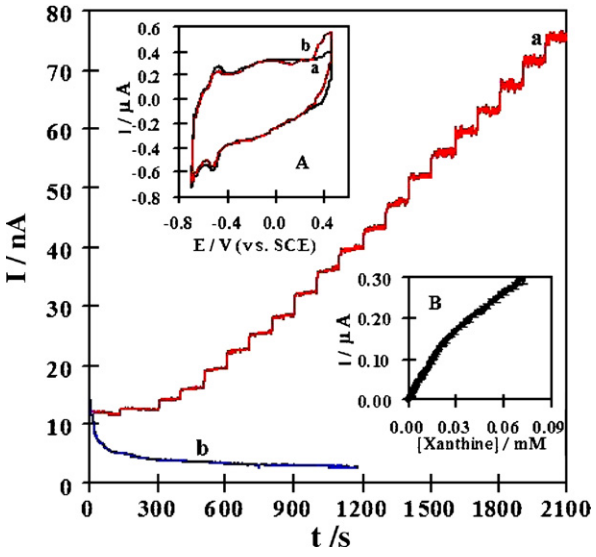

Fig. 4. Steady-state responses of XnOx/laponite/GCE on successive injection of xanthine into 10 ml of stirring 0.1 M PBS. Applied potential, 0.39 V. Inset A: Cyclic voltammograms of a XnOx/laponite/GCE in PBS with pH 7.5 containing (a) no xanthine and (b) 20 μM xanthine. The scan rate was 150 mV s^{-1}. Inset B: Calibration curve of XnOx/laponite/GCE.

3.4. Electrocatalytic behavior of XnOx/laponite/GCE

3.4.1. Catalysis to xanthine

The catalytic properties of XnOx/laponite/GCE to xanthine were investigated by cyclic voltammetry in PBS (pH 7.5). Upon addition of 20 μM xanthine to the electrochemical cell, a pronounced catalytic wave emerges at ca. +390 mV vs. SCE (curve b of Fig. 4 inset A). The maximum current rises with increasing xanthine concentration (data not shown). In the absence of XnOx, it has been well established that xanthine is electro-inactive within this potential range. Moreover, FAD/laponite has no either the catalysis to xanthine within the same potential range. The observed current is due to an electrochemically driven enzymatic oxidation of xanthine. In principle, at potentials positive of −0.4 V (Inset A of Fig. 4), all redox-active centers in XnOx are fully oxidized and hence the enzyme should be catalytically active. However, catalysis does not begin until the electrode potential reaches 0.39 V. This is an apparent over-potential of almost 880 mV relative to the FAD couple; the site at which the natural electron acceptor binds. This is reminiscent of the large anodically shifted catalytic wave reported by Bernhardt et al., proposed that an (inactive) 2-electron reduced form of the Mo cofactor is present below the catalytic potential that bears a ring-opened tetrahydropterin, and that the electrochemically driven catalytic cycles is contingent on an oxidative ring closure (Aguey-Zinsou et al., 2003).

The electrocatalytic reaction of xanthine at XnOx/laponite/GCE was also studied by amperometry, which is one of the most widely employed techniques for biosensor. The applied potential of 0.39 V (vs. SCE) was chosen as the applied potential for the amperometric determination of xanthine. Fig. 4 shows the typical response curves for the XnOx/laponite/GCE (curve a) and laponite/GCE (curve b) on successive injections of xanthine to a stirred PBS (pH 7.5), respec-

Table 1
Comparison analytical performance of other xanthine biosensor.

Electrode	E_{app} (V)	Linear range (M)	Sensitivity (mA M^{-1})	DL (μM)	Rep (RSD)	References
CoPc/BTM/CPE	0.35	1×10^{-3}–1.5×10^{-2}	–	1	10.26%	Kilinc et al. (1998)
PPY/XnOx	−0.15	1×10^{-6}–2×10^{-5}	0.19	–	–	Liu et al. (2004)
PPY/Au/XnOx			0.44	–	–	
XnOx/Poly-TTCA	0.30	5.0×10^{-6}–1.0×10^{-4}		1	7.5%	Rahman et al. (2007)
	−0.35	5.0×10^{-7}–1.0×10^{-4}	5.35	0.09	6.7%	
XnOx/GCP	0.9	5.0×10^{-7}–4.0×10^{-5}	–	0.1	4.12%	Kirgöz et al. (2004)
XnOx–CD–CMC–ADA–Au	0.7	3×10^{-4}–1.04×10^{-2}	0.25	200	–	Villalonga et al. (2007)
XnOx/LDHs/GCE	0.55	1.0×10^{-6}–2.0×10^{-4}	15.4	0.1	4.5%	Shan et al. (2009a)
XnOx/$CaCO_3$	0.55	2×10^{-6}–2.5×10^{-4}	12.0	2	4.8%	Shan et al. (2009b)
XnOx/HRP/$CaCO_3$	−0.05	4×10^{-7}–5×10^{-5}	–	0.1	–	
XnOx/laponite	0.39	3.9×10^{-8}–2.1×10^{-5}	6.54	0.01	2.7%	This work

CoPc: Cobalt phthalocyanine; BTM: buttermilk; PPY: poly-pyrrole; poly-TTCA: poly-5,2″:5′,2″-terthiophine-3-carboxylic acid; CD–CMC: β-cyclodextrins-branched carboxymethyl cellulose; ADA: 1-adamantane; LDHs: layered double hydroxides.

tively. At a laponite/GCE without immobilized XnOx, no current was observed by addition of xanthine (curve b in Fig. 4). However, with a XnOx/laponite/GCE, a stepped growth of oxidation current was observed with stepped increase of xanthine concentration in buffer solution (curve a in Fig. 4), showing that XnOx can catalyze the oxidation of xanthine. The inset B in Fig. 4 shows the calibration curve obtained via the XnOx/laponite/GCE. A clearly defined oxidation current proportional to the concentration of xanthine was observed. The biosensor achieved 95% of the steady-state current within 5 s, with a linear range of 3.9×10^{-8} to 2.1×10^{-5} M. The detection limit was 1.0×10^{-8} M based on S/N = 3. The apparent Michaelis–Menten constant (K_M^{app}) can be obtained by the analysis of the slope and the intercept of the plot of the reciprocals of the steady-state current versus xanthine concentration. K_M^{app} value for XnOx/laponite film modified GCE was found to be 6.4×10^{-5} M. This value is close to the reported for the free XnOx (4.5×10^{-5} M), illustrating the non-denaturating character of the enzyme immobilization with laponite nanoparticles.

The analytical performances of the proposed xanthine sensor were compared with other xanthine sensing systems based on oxidation or reduction of enzymatically generated H_2O_2, as summarized in Table 1. It appears that the XnOx/laponite/GCE exhibits the relatively low detection limit, high sensitivity and satisfactory reproducibility.

At the applied potential of 0.39 V, interferences were evaluated by intercalation of four interferents: 5 mM glucose, 2 mM sodium benzoate, 0.01 mM ascorbate and 0.02 mM L-cysteine. No appreciable signals were observed for the successive injections of interferents into the electrolyte solution. On the other hand the addition of 12.8 μM xanthine, provided a response closed to that determined in the absence of interferents. This non-significant interference effect is probably due to the efficiency of the electrocatalytic process, which permits the amperometric detection of xanthine at 0.39 V vs. SCE.

3.4.2. Catalysis to nitrate

Assimilatory nitrate reductase (NR, EC 1.6.6.1) catalyzes the rate-limiting and regulated step, the reduction of nitrate to nitrite, in the pathway of inorganic nitrogen assimilation (Solomonson and Barber, 1990). The active centers of NR contain also FAD, Mo and Fe–S clusters. Since XnOx shares the similar structure to that of NR, nitrate catalytic reduction by this proposed XnOx/laponite/GCE was also investigated using cyclic voltammetry in PBS (pH 5.0). Fig. 5 shows the CVs of XnOx/laponite/GCE in the absence or in the presence of nitrate. The pair of well-defined peaks about −0.365 V is attributed to XnOx–FAD/XnOx–$FADH_2$ redox couple. On introduction of nitrate to the electrochemical cell, a slight increase in reduction peak current and a slight decrease in the oxidation peak current at about −0.365 V are observed simultaneously (curve b to h in Fig. 5), and a new reduction wave appears around −0.75 V, the wave height increases with a further addition of KNO_3. In contrast, no catalytic current is observed within an identical potential range at laponite/GCE. It indicates that the reduction of nitrate is catalyzed by the XnOx/laponite/GCE. The electrons may be delivered to the active site of XnOx (Mo center) in an intramolecular process: from the electrode, flavin prosthetic group, Fe–S clusters and finally migrate to nitrate via the Mo center (Anderson et al., 2001). Inset of Fig. 5 presents the resulting calibration curve of ΔI_{peak} versus nitrate concentration. The XnOx/laponite/GCE response was linear with nitrate concentration from 2×10^{-5} to 3×10^{-4} M, with the linear regression equation being $\Delta I_{pc} = -0.0646 - 3.643C$ ($R^2 = 0.9945$, C in mM, ΔI_{pc} in μA).

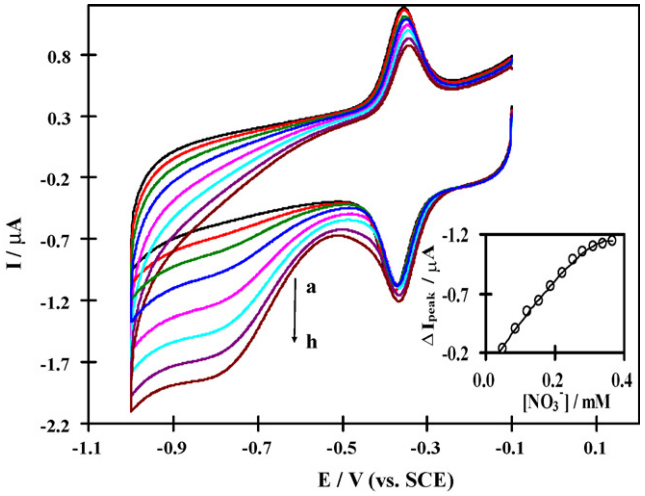

Fig. 5. Cyclic voltammograms of XnOx/laponite/GCE in 0.1 M PBS (pH 5.0) containing no nitrate (a), 0.0196 M nitrate (b), 0.0484 M nitrate (c), 0.0851 M nitrate (d), 0.155 M nitrate (e), 0.220 M nitrate (f), 0.310 M nitrate (g) and 0.336 M nitrate (h). Inset: Dependence of the increased reduction peak current of XnOx/laponite/GCE at −0.75 V on the concentration of nitrate in 0.1 M PBS (pH 5.0).

4. Conclusion

Herein we provide another successful example to demonstrate that laponite nanopartiles as also promising materials in the construction the third-generation biosensor. Nanosized laponite particles can provide a high specific surface area to the large amount of protein loading; its high surface energy can lead the conformational change of protein molecules favorable to the direct electron transfer between the protein molecules and the underlying electrode; its high hydrophilic property can help the immobilized proteins retain their native biological activity. Thus,

XnOx/laponite/GCE exhibited direct electrochemical behavior and excellent electrocatalytic activities to several substrates based on the active Mo centers.

Acknowledgements

The authors are grateful to the financial supports of National Natural Science Foundation of China (Grant NO. 20505014 20810102052, 20705030 and 20773108), Qing Lan Project and the project sponsored for D. Shan by the scientific research foundation for the returned overseas Chinese scholars, state education ministry. S.-N. Ding is grateful to the "Foundation Franco-Chinoise pour la Science et ses Applications" (FFCSA) for the postdoctoral fellowship and the Natural Science Foundation of Jiangsu (BK2007563) for financial support.

References

Aguey-Zinsou, K.F., Bernhardt, P.V., Leimkühler, S., 2003. J. Am. Chem. Soc. 125, 15352–15358.
Anderson, L.J., Richardson, D.J., Butt, J.N., 2001. Biochemistry 40, 11294–11307.
Bernhardt, P.V., Honeychurch, M.J., McEwan, A.G., 2006. Electrochem. Commun. 8, 257–261.
Bonn, D., Kellay, H., Tanaka, H., Wegdam, G., Meunier, J., 1999. Langmuir 15, 7534–7536.
Cosnier, S., Le Lous, K., 1996. J. Electroanal. Chem. 406, 243–246.
Cosnier, S., Mousty, C., Gondran, C., Lepellec, A., 2006. Mater. Sci. Eng. C 26, 442–447.
Cummins, H.Z., 2007. J. Non-Cryst. Solids 353, 3891–3905.
Eger, B.T., Okamoto, K., Enroth, C., Sato, M., Nishino, T., Pai, E.F., Nishino, T., 2000. Acta Cryst. D 56, 1656–1658.
Fan, Q., Shan, D., Xue, H.G., He, Y.Y., Cosnier, S., 2007. Biosens. Bioelectron. 22, 816–821.
Freire, R.S., Pessoa, C.A., Mello, L.D., Kubota, L.T., 2003. J. Braz. Chem. Soc. 14, 230–243.
Harrison, R., 2002. Free Rad. Biol. Med. 33, 774–794.
Hille, R., 2005. Arch. Biochem. Biophys. 433, 107–116.
Joshi, Y.M., Reddy, G.R.K., Kulkarni, A.L., Kumar, N., Chhabra, P.R., 2008. Proc. R. Soc. A 464, 469–489.
Kilinc, E., Erdem, A., Gokgunnec, L., Dalbasti, T., Karaoglan, M., Ozsoz, M., 1998. Electroanalysis 10, 273–275.
Kirgöz, Ü.A., Timur, S., Wang, J., Telefoncu, A., 2004. Electrochem. Commun. 6, 913–916.
Laviron, E., 1979. J. Electroanal. Chem. 100, 263–270.
Li, Z., Hu, N., 2003. J. Electroanal. Chem. 558, 155–165.
Liu, Y., Nie, L., Tao, W., Yao, S., 2004. Electroanalysis 19, 1271–1278.
Liu, Y., Liu, H., Hu, N., 2005a. Biophys. Chem. 117, 27–37.
Liu, X., Peng, W., Xiao, H., Li, G.X., 2005b. Electrochem. Commun. 7, 562–566.
Ma, K., Chung, T., Good, R.J., 1998. J. Polym. Sci. Pol. Phys. 36, 2327–2337.
Mousty, C., Cosnier, S., Shan, D., Mu, S.L., 2001. Anal. Chim. Acta 443, 1–8.
Rahman, M.A., Won, M.S., Shim, Y.B., 2007. Electroanalysis 19, 631–637.
Rodrigues, C.G., Wedd, A.G., 1991. J. Electroanal. Chem. 312, 131–140.
Senillou, A., Jaffrezic, N., Martelet, C., Cosnier, S., 1999. Anal. Chim. Acta 401, 117–124.
Shan, D., Mousty, C., Cosnier, S., Mu, S.L., 2002. J. Electroanal. Chem. 537, 103–109.
Shan, D., Mousty, C., Cosnier, S., Mu, S.L., 2003. Electroanalysis 15, 1506–1512.
Shan, D., Han, E., Xue, H.G., Cosnier, S., 2007. Biomacromolecules 8, 3041–3046.
Shan, D., Wang, Y., Zhu, M., Xue, H.G., Cosnier, S., Wang, C., 2009a. Biosens. Bioelectron. 24, 1171–1176.
Shan, D., Wang, Y.N., Xue, H.G., Cosnier, S., 2009b. Sensor Actuat. B-Chem. 136, 510–515.
Shi, Q.F., Li, Q.B., Shan, D., Fan, Q., Xue, H.G., 2008. Mater. Sci. Eng. C 28, 1372–1375.
Shumyantseva, V.V., Ivanov, Y.D., Bistolas, N., Scheller, F.W., Archakov, A.I., Wollenberger, U., 2005. Anal. Chem. 76, 6046–6052.
Solomonson, L.P., Barber, M.J., 1990. Annu. Rev. Plant. Physiol. Mol. Biol. 41, 225–253.
Sun, H., 2006. J. Porous Mater. 13, 393–397.
Van Olphen, H., 1977. An Introduction to Clay Colloid Chemistry. Wiley, New York, NY.
Villalonga, R., Matos, M., Cao, R., 2007. Electrochem. Commun. 9, 454–458.
Wang, L., Yuan, Z., 2004. Anal. Sci. 20, 635–638.
Wu, Y., Hu, S., 2007. Anal. Chim. Acta 602, 181–186.
Zhao, J., O'Daly, J.P., Henkens, R.W., 1996. Biosens. Bioelectron. 11, 493–502.
Zhou, Y., Hu, N., Zeng, Y., Rusling, J.F., 2002. Langmuir 18, 211–219.
Zhou, H., Xu, Y., Chen, T., Suzuki, I., Li, G.X., 2006. Anal. Sci. 22, 337–340.